Korean J. Chem. Eng., 38(6), 1277-1290 (2021)
DOI: 10.1007/s11814-021-0830-4

pISSN: 0256-1115
eISSN: 1975-7220

Synthesis, characterization of novel Fe-doped TiO_2 activated carbon nanocomposite towards photocatalytic degradation of Congo red, *E. coli*, and *S. aureus*

Mridushmita Baruah*, Soremo Likongthung Ezung*, Aola Supong*, Parimal Chandra Bhomick, Suraj Kumar*, and Dipak Sinha*,†**

*Department of Chemistry, Nagaland University, Lumami-798627, Nagaland, India
**Department of Chemistry, Immanuel College, Dimapur-797112, Nagaland, India
(*Received 14 January 2021 • Revised 10 April 2021 • Accepted 29 April 2021*)

Abstract−In this work, the synthesis, characterization, and photocatalytic activity of iron-doped titanium dioxide nanoparticles (FDT) supported on environmentally benign activated carbon (PAC) has been discussed. The photocatalytic activity of the nanocomposite was investigated for the degradation of Congo red (CR) dye from aqueous solution under visible light (520 nm), and it was observed that 100% degradation for 20 ppm CR solution took place within 60 mins. The experimental data of photodegradation of CR using the FDT/PAC nanocomposite had the highest correlation with Langmuir Hinshelwood model and pseudo-first-order rate kinetics with an apparent rate constant of 0.05341 min^{-1} and half-life period of 12.97 mins, respectively. The thermodynamics study revealed that the degradation process is exothermic and spontaneous. The effect of interfering ions on the degradation of CR solution was also examined. The photocatalytic antibacterial activity of the nanocomposite was tested against two bacteria pathogens, *Escherichia coli* and *Staphylococcus aureus*, and it was found that for the concentration of 10^5 CFU ml^{-1}, 100% photocatalytic inactivation was achieved for both *Escherichia coli* in 120 mins and *Staphylococcus aureus* in 75 mins under visible light irradiation. The total electrical energy consumed and operating cost were measured and the total operating cost was 312.50, 236.74, and 166.67 INR (Indian rupee) for 20 ppm, 60 ppm, and 100 ppm CR dye removal using 0.06 g FDT/PAC nanocomposite, respectively.

Keywords: FDT/PAC Nanocomposite, Photodegradation, Congo Red Dye, Antibacterial Activity, Electric Energy Per Order

INTRODUCTION

The impact of nanotechnology has become increasingly evident in different areas of science and technology, including environmental remediation and disinfection. Several environmentally beneficial technologies, such as heterogeneous photocatalysis (HP) and solar disinfection (SODIS) using metal oxide semiconductor photocatalysts, have been developed and applied extensively for air purification, wastewater treatment, and environmental regulations [1-3]. Among all the metal oxides used, TiO_2 is the most potential photocatalyst due to its chemical constancy, low cost, less harm, photochemical stability, and no further requirement of secondary disposal and expensive oxidizing chemicals. However, a high quantity recombination rate between electron and hole pairs limits the use of TiO_2 in the visible region (400-750 nm), which accounts for 43% of solar light [4]. Therefore, to overcome this problem, it is desired to alter the band structure of the anatase TiO_2 and, in this regard, different methodologies like metal/non-metal elements doping, dye photosensitization, hydrogen treatment have been developed to enhance the TiO_2 photoactivity in the visible light region [4]. Among different alterations, transition metal doping is a simple and efficient approach to widen the wavelength region of TiO_2 to the visible light range [5]. The use of dopant in the metal oxide creates an intermediate level in the lattice which constrains the electron-hole pair to recombine, and hence the recombination rate decreases and ultimately the photocatalytic activity of TiO_2 gets enhanced [6]. Among the different metal dopants, Fe^{3+} has garnered more attention due to its ionic radius of 0.64 Å, which is identical to the ionic radius of Ti^{4+} (0.68 Å); therefore, making it easier to substitute Fe^{3+} into the crystal structure of TiO_2. Application of Fe doped in TiO_2 has been widely reported for the degradation of environmental pollutants [7-9], NO_x removal [4], CO_2 reduction [10], and water splitting for hydrogen production [11]. Literature reports have showed that the incorporation of Fe^{3+} ions in the TiO_2 lattice reduces the electron-hole recombination rate, narrows the TiO_2 band gap, and thus increases the photocatalytic activity of TiO_2. However, powdered TiO_2 has low exchange efficacy and is difficult to split after the photocatalytic reaction [7]. Hence to achieve quick and easy degradation of organic pollutants and also for simple management of the photocatalyst, it is desired that TiO_2 be loaded onto an appropriate adsorbent. In this regard, different adsorbents such as zeolites, perlite, clay, silica, and activated carbon have been used as support systems for TiO_2 [12]. Activated carbon with good adsorption capacity is more appropriate as an adsorbent support system for the photocatalyst in any wastewater treatment process, as it can significantly gather pollutant molecules near the photocatalytic sites during the adsorption-degradation process. Additionally, the synergistic effect between activated carbon and TiO_2 will separate the

†To whom correspondence should be addressed.
E-mail: dipaksinha@gmail.com

photo-induced electrons and electrons-holes and inhibit their rapid recombination, which extends the electron's life-time and a likelihood of increased photocatalytic efficiency.

Wide use of toxic dyes in fabric production can cause ecological degradation and human sickness [13]. Dyes in wastewater is a major cause of water contamination and interferes with the oxygen transport system at the water-air interface [14]. Among the toxic dyes, Congo red is the most commonly used in fabric production, and it consists of various benzidine groups which are carcinogenic and mutagenic [15]. Therefore, through this work, an effort has been made to remove this dye with Fe-doped TiO_2 activated carbon nanocomposite and the results are presented in detail.

The presence of pathogenic microbes such as *Escherichia coli* (*E. coli*) and *Staphylococcus aureus* (*S. aureus*) in ambient water is also a major concern throughout the world because they cause water-borne diseases. Different methods that have been employed to control microbes, including pasteurization, ultra-high pressure/temperature treated sterilization, and, microwave sanitization [16]; however, most of them require heat treatment and thus have limitations. Hence an alternative method using metal oxide nanoparticle has been studied for the inactivation of microbes. Metal oxide photocatalysis is employed for not only the removal of organic contaminants but also for inactivating different microbes in wastewater. The main reason for using photocatalysis is that the reactive oxygen species, produced during photocatalysis, can kill the microbes through nucleic acid attack, co-enzyme oxidation, and by dis-organizing cell membrane [17]. Visible light driven photocatalytic inactivation of microbes by metal doped TiO_2 photocatalyst [18], carbon supported metal oxide nanocomposite [19], and metal co doped TiO_2 [17] were investigated by many researchers in the last decades. Veréb et al. reported the bare and doped rutile and anatase TiO_2 photocatalyst for photocatalytic inactivation of *E. coli* in water under visible light irradiation [20]. Masae et al. introduced a photocatalytic inactivation of *E. coli* in water using Se doped TiO_2 under visible light irradiation [21]. Hence, metal modified TiO_2 has received much attention due to its extended visible light absorption efficacy.

Therefore, in the present study, we prepared visible light active FDT/PAC nanocomposite via a combination of ultrasonic-hydrothermal treatment to ensure good dispersion of Fe doped TiO_2 on activated carbon surface to generate a high photocatalytic activity. Standard characterization protocols were employed to understand the basis of the improved activity of the nanocomposite. The photocatalytic inactivation property of the nanocomposite was also explored against gram-positive and gram-negative bacteria. The typical mechanisms for the photodegradation of Congo red and photocatalytic inactivation of bacteria are shown in Scheme 1. This could be one of the first reports to highlight the use of FDT/PAC nanocomposite for degradation of anionic Congo red dye from wastewater using less amount of nanocomposite, reaction time, and secondly, this nanocomposite was also used as an antimicrobial for the inactivation of microbes. The operating cost and electrical energy consumed while conducting the experiment were calculated and found to be minimal using FDT/PAC nanocomposite.

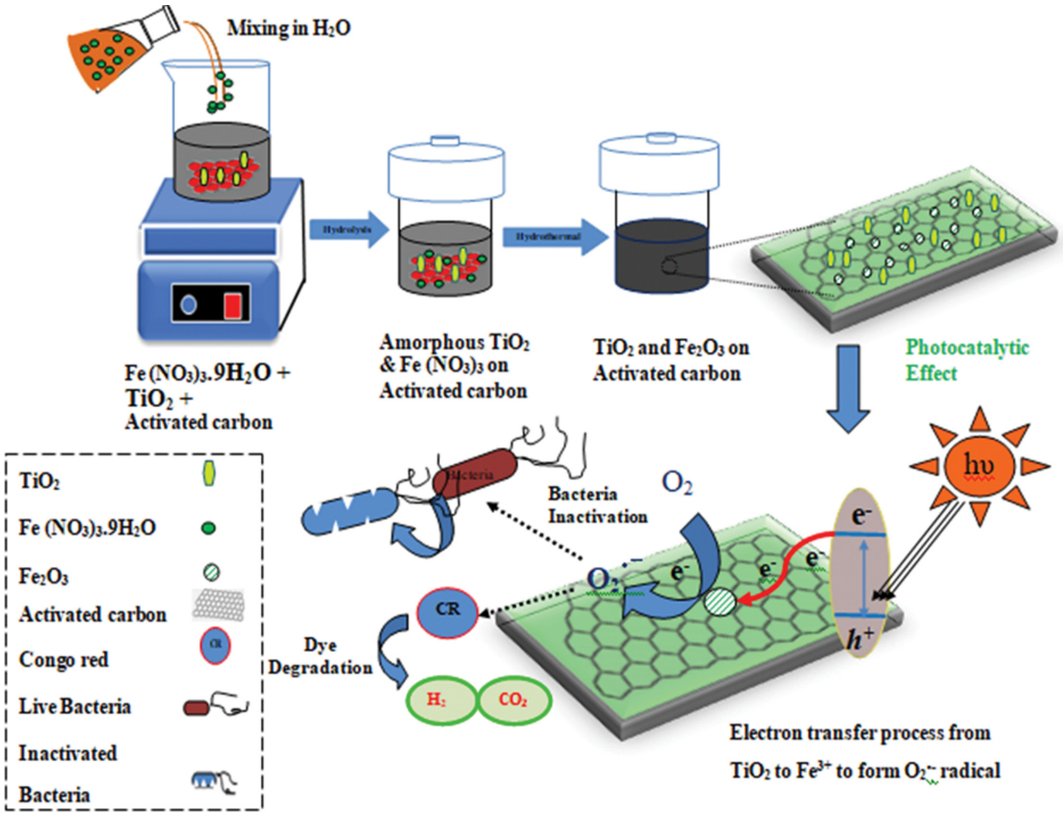

Scheme 1. Schematic illustration of photodegradation of Congo red and photocatalytic inactivation of bacteria over FDT/PAC nanocomposite.

EXPERIMENTAL SECTION

1. Materials

Titanium tetrachloride ($TiCl_4$, 99.10%), Congo red (CR), ferric nitrate (98%), zinc chloride (99%), sulfuric acid (98%), and ammonia (25%) were supplied from Sigma-Aldrich. Co., India. All chemicals utilized were of pure scientific grade and used without further purification.

2. Synthesis of FDT/PAC Nanocomposite

For the synthesis of FDT/PAC nanocomposite, activated carbon and TiO_2 were used as precursors. Bio waste pinecones were utilized for activated carbon preparation and the sol-gel method was used for the synthesis of TiO_2 nanoparticles. The synthetic route for the preparation of pine cone activated carbon (PAC) with photocatalyst TiO_2 was reported in one of our earlier research papers [22].

In the synthesis of FDT/PAC nanocomposite, 0.15 g of the as-prepared sol-gel TiO_2 nanoparticle was slowly added to 1 g of 100 ml ferric nitrate solution and the solution was simultaneously stirred for 30 mins. Thereafter, 0.3 g of the as-prepared PAC was poured slowly into the above mixture and the obtained solution was ultrasonicated for 1 h. Later, the sonicated mixture was shifted into a hydrothermal autoclave and kept at 150 °C inside the oven for 24 h. After the hydrothermal treatment the solution was washed appropriately with double refined water using a centrifuge machine so that solution pH became neutral and finally the solution was dried at 65 °C for 12 h [23].

3. Characterization of FDT/PAC Nanocomposite

The crystal structure of the FDT/PAC nanocomposite was obtained using an X-ray diffractometer (X'pert PRO, Philips, Japan, CuKα radiation). The surface structure of the TiO_2, TiO_2/pinecone activated carbon (TiO_2-NP/PAC,) and FDT/PAC nanocomposite was studied using scanning electron microscopy (SEM, Zeiss, Sigma-300). Elemental analysis was done using energy-dispersive X-ray spectroscopy (EDX). The functional groups present on the FDT/PAC nanocomposite were identified using Fourier transform infrared (FT-IR) spectrometer (Model: Spectrum Two, Made: Perkin Elmer). The band gap energy was studied using a diffuse reflectance spectrophotometer (DRS, Shimadzu, and wavelength 200-600 nm). Photoluminescence spectrophotometer (Horiba Fluoromax-4CP spectrofluorometer, 150 W Xenon Lamp) was used to obtain the photoluminescence (PL) spectra. Surface areas of the samples were measured by the N_2 adsorption-desorption isotherm with a Quantachrome instrument (Autosorb iQ Station 1, 77 K) based on the Brunauer-Emmett-Teller (BET) model. The total pore volume and pore radius were estimated from the consequent N_2 adsorption volume via the Barrett-Joyner-Halenda (BJH, at relative pressure 0.09) theory. The batch equilibrium method was used to determine the zero-point charge (pH_{zpc}) of the FDT/PAC nanocomposite [24]. For pH_{zpc} measurement, 50 ml of $NaNO_3$ (0.1 M) was mixed with 0.1 g of FDT/PAC nanocomposite, and the starting pH values were adjusted between 1-11 by adding either 0.1 M HCl or NaOH solution. Afterward, the solutions were continuously stirred for two days using a magnetic stirrer and the final pH of each solution was measured. The variation among the initial and final pH values ($\Delta pH = pH_{initial} - pH_{final}$) was plotted against $pH_{initial}$ value of the FDT/PAC nanocomposite solution.

4. Photocatalytic Degradation Experiment

A photocatalytic reactor was used to perform the photocatalytic reaction of CR, which consists of a black box (dimension: 63×44×44 cm). A 250 ml Pyrex glass vessel containing 200 ml of CR solution was placed above a magnetic stirrer and an amount of FDT/PAC was mixed with the solution at the bottom of the reactor. A visible lamp having a maximum wavelength of 520 nm (High-pressure mercury lamp, 350 W) was located at the top of the reactor, 10 cm away from the reaction solution. The photocatalytic reaction was caused by the use of visible radiation which reached the FDT/PAC photocatalyst through the pollutant solution. The reactor temperature was maintained at 25 °C using a constant flow of water inside the reaction scheme using a water pump. Also, an exhaust fan was used inside the reactor for the continuous circulation of air.

For the degradation of CR dye, a stock solution of CR (1,000 ppm) was first prepared using 1 g of CR in 1,000 ml double refined water. Further, the required concentration was obtained by the dilution of stock solution to various concentrations 20 ppm, 60 ppm, and 100 ppm. For this study, FDT/PAC nanocomposite was mixed in 200 ml CR dye solution of varied concentration (20 ppm, 60 ppm, and 100 ppm) by vigorously stirring the reaction mixture without exposure to light till 30 min so that adsorption-desorption equilibrium could be established within the reaction system. After equilibrium was established, the concentration of the dye was measured, and this was taken as the initial concentration so that the adsorption of CR due to the nanocomposite did not hinder the study of the overall photocatalytic effect. Later, the final concentration of the dye solution was measured using a UV-Vis spectrophotometer at λ_{max} of 497 nm by taking out 3.5 ml at every 10 min interval.

The CR degradation percentage was calculated by Eq. (1):

$$\text{CR degradation}\ (\%) = \frac{C_o - C_e}{C_0} \times 100 \tag{1}$$

where C_o and C_e are the concentrations of CR before and after the photocatalytic treatment.

5. Antibacterial Activity Experiment

For the photocatalytic antimicrobial test of FDT/PAC nanocomposite, gram-negative bacteria *Escherichia coli* (*E. coli*) and gram-positive bacteria *Staphylococcus aureus* (*S. aureus*) were used as test bacterium. *E. coli* and *S. aureus* were cultured using Luria-Bertain (LB) nutrient broth and the solution was incubated for 6 h at 37 °C overnight. The bacterial pellet was assembled by centrifuging the culture medium at 2,500 rpm for 15 min and suspended in the autoclaved distilled water. The initial concentration was adjusted to 10^5 CFU (colony forming unit) ml^{-1}. The nutrient agar and broth media, and all plating equipment were autoclaved before starting the experiments.

5-1. Photocatalytic Inactivation Procedure

The photocatalytic reactor described in section 4 of the experimental section was used for the photocatalytic inactivation study of bacteria. At first, autoclaved nutrient agar was poured into Petri plates for solidification. Then, 70 ml of bacterial suspension (10^5 CFU ml^{-1}) was added to the sterile Pyrex glass vessel and was

stirred using a magnetic stirrer (150 rpm) throughout the experiments. Thereafter, 0.05 g of the nanocomposite was added and the resultant mixture was exposed to visible light. At specified time intervals, 0.01 ml of the suspension was collected from the reactor and spread on the nutrient agar plates. To cultivate the bacteria, the agar petri plates were placed inside an incubator at 37 °C for 24 h. After incubation, the bacteria residual colonies were quantified using a digital colony counter.

The photocatalytic inactivation efficiency of bacteria was calculated using Eq. (2) [25]:

$$\text{Inactivation efficiency (\%)} = \frac{\text{no. of colonies} \times \text{dilution factor}}{\text{volume of culture plate}} \quad (2)$$

RESULTS AND DISCUSSION

1. Characterization of FDT/PAC Nanocomposite

XRD peaks of FDT/PAC nanocomposite are shown in Fig. 1 and a comparison is made with the XRD peaks of TiO_2, TiO_2-NP/PAC [22].The XRD peaks at 2θ=25.281, 38.576, 48.050, 53.891, 55.062, 62.690, 68.762, 70.311 and 75.032 correspond to (1 0 1), (1 1 2), (2 0 0), (1 0 5), (2 1 1), (2 0 4), (1 1 6), (2 2 0) and (2 1 5) planes, which confirms that the samples have anatase crystalline form of TiO_2 (JCPDS 21-1272). The peaks related to Fe ions are not found in the XRD pattern of FDT/PAC nanocomposite. This observation can be ascribed to the fact that Fe ions were incorporated into the crystal lattice of titania due to the similar radius of Ti^{4+} (0.068 nm) and Fe^{3+} (0.064 nm) [8]. It is believed that Fe^{3+} inserts into the interior matrix of the Fe doped TiO_2 nanoparticles instead of exterior surface [26]. Similar patterns of results i.e., absence of Fe signal in XRD spectra for Fe doped TiO_2 were also observed by several other authors [6,27,28], and [29]. Furthermore, no XRD phase was found for activated carbon due to its amorphous structure. The crystalline size calculated for the FDT/PAC nanocomposite using the Debye-Scherer equation was found to be 4.36 nm.

The SEM micrograph of the FDT/PAC nanocomposite is shown in Fig. 2(a). From the SEM image of FDT/PAC nanocomposite, it can be observed that white spherical particles of TiO_2 with different sizes were irregularly agglomerated on the surface of the PAC, and there were fine Fe ions accumulated or attached to the surface of the TiO_2. The presence of Fe ions on the surface of the PAC is expected to increase the absorption of light in the visible light region, thus enhancing the photocatalytic activity. Furthermore, the Fe doped TiO_2 nanoparticles are well dispersed on the PAC surface and have an average 2-20 nm particle size distribution.

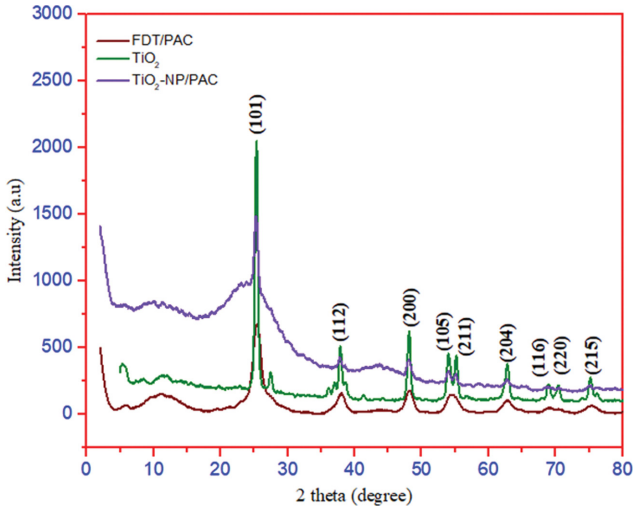

Fig. 1. X-ray diffraction pattern of FDT/PAC nanocomposite and a comparison with TiO_2, TiO_2-NP/PAC [22].

The purity and elemental composition of the FDT/PAC nanocomposite were analyzed by EDX analysis (Fig. 2(b)). The EDX spectrum revealed that the FDT/PAC nanocomposite has a Fe content of 29.27%, Ti of 28.69%, C of 2.52%, and O of 28.22%, which confirms the equal distribution of Fe, Ti, and O over the C surface.

FT-IR spectra of the TiO_2 and FDT/PAC nanocomposite are shown in Fig. 3. The peaks of the TiO_2 and FDT/PAC nanocomposite at 3,500 cm^{-1} and 1,600 cm^{-1} are assigned due to the stretching and bending vibrations of the O-H and H-O-H bond, which can be attributed to the physically and chemically absorbed sur-

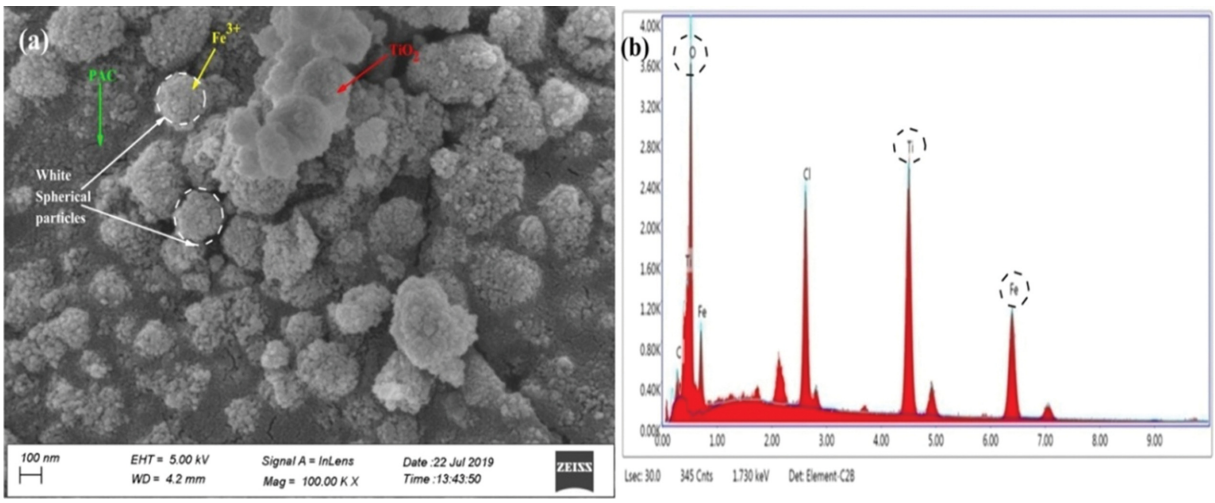

Fig. 2. (a) SEM image of FDT/PAC nanocomposite, (b) EDX spectra of FDT/PAC nanocomposite.

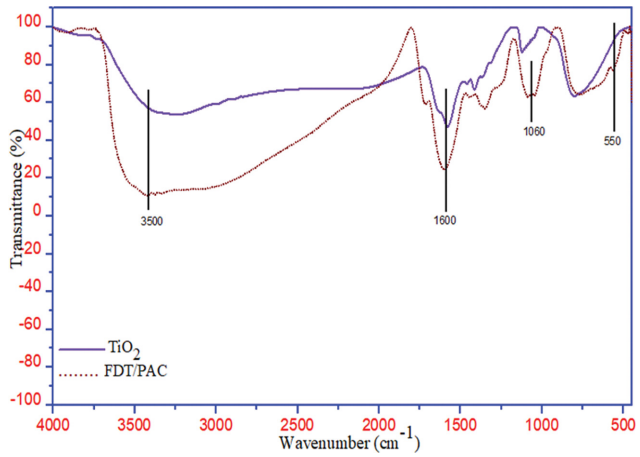

Fig. 3. FT-IR spectra of TiO_2 and FDT/PAC nanocomposite.

face water. The peak at around 550 cm^{-1} is related to the stretching vibration of the Ti-O bond [30]. A new peak at 1,060 cm^{-1} appeared for the FDT/PAC nanocomposite, which confirms the presence of stretching vibration of the Ti-O-C bond [8]. This suggests that the TiO_2 nanoparticles were attached chemically with the C surface and hence Ti cannot be easily separated from the C surface.

The UV-Vis DRS spectra of Fe doped nanocomposite (FDT/PAC) and TiO_2, are shown in Fig. 4 and compared with TiO_2-NP/PAC [22]. From Fig. 4(a), it can be observed that the absorption peak of TiO_2 and TiO_2-NP/PAC appears in the wavelength range between 200-380 nm, which is in the ultra-violet light region. On the other hand, in the FDT/PAC nanocomposite, the absorption edge shifts towards the visible light region that is a wavelength range between 400-800 nm due to the doping of Fe ion. The absorption peak of TiO_2 in the UV range appears due to the transition from the 2p level of O to the 3d level of Ti. With Fe doping, the absorption peak of FDT/PAC nanocomposite shifted to a longer wavelength due to the excitation of the 3d electron of Fe^{3+} ion to the conduction band of TiO_2 [8]. The optical band gap energy was calculated using Tauc's equation given below:

$$\alpha h\nu = K(h\nu - Eg)^n \quad (3)$$

where, Eg=optical band gap, $h\nu$=photon energy, α=molar extinction coefficient, K is the proportionality constant, and n depends on the type of transition.

From the $(\alpha h\nu)^2$ vs $h\nu$ curve, the Eg values of the FDT/TiO_2 nanocomposite and TiO_2 were found to be 2.3 and 3.1 eV as compared to, TiO_2-NP/PAC, i.e., 3.2 eV [22]. It can be seen from Fig. 4(b) that the Eg value of the TiO_2 decreased from 3.1 to 2.3 eV with the addition of Fe ions in the FDT/PAC nanocomposite, which improved the absorption of light in the visible region.

The efficiency of separation of photogenerated electron-hole pair can be investigated using photoluminescence (PL) spectra. The lesser the PL peak intensity, the lesser the affinity to recombine the electron-hole pair, which leads to more electron-hole pair participation in the photochemical reaction, thus increasing the photocatalytic activity of the nanocomposite. In this present study, the PL spectra of TiO_2 and FDT/PAC nanocomposite are analyzed in the wavelength range from 450-750 nm (Fig. 5). The sharp emission peak at 468 nm in the TiO_2 is due to the transition of charge from Ti3d to the O 2p level and signifies the recombination of the electron-hole pair [31]. Similar results have also been observed by Hasibur et al. [32], which showed that the PL emission peak of TiO_2 comes at around 477 nm wavelength, indicating the band-gap recombination of electron-hole pair. The PL peak intensity for FDT/PAC nanocomposite was found to decrease as compared to TiO_2, which confirms that the recombination of the electron-hole pair reduced significantly in the nanocomposite as compared to TiO_2. This is due to the formation of a dopant energy level (Fe^{3+}/Fe^{4+}) within the bandgap of TiO_2 (nearer the valance band), which results in the excitation of Fe^{3+} 3d-electrons from the dopant energy level to the TiO_2 conduction band (CT transition) [33]. Hence, the presence of Fe ions in the composite decreases the electron-hole recombination by increasing the lifetime of the charge carrier, which is expected to improve the photocatalytic activity.

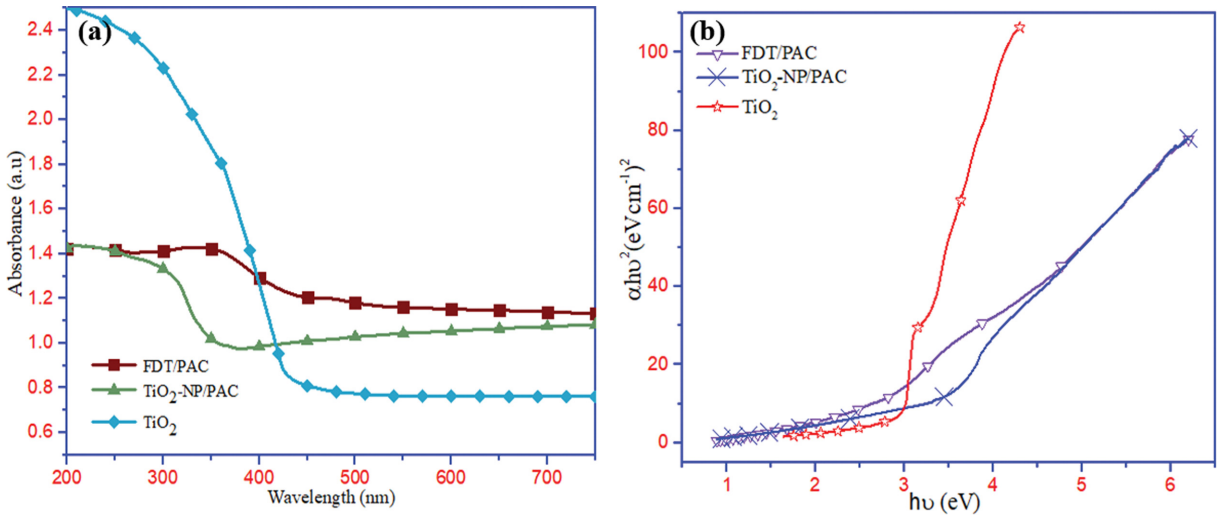

Fig. 4. (a) UV-Visible DRS spectra and (b) Tauc plot for the determination of optical band gap for TiO_2 and FDT/PAC nanocomposite, (plot for TiO_2-NP/PAC is shown for comparison only) [22].

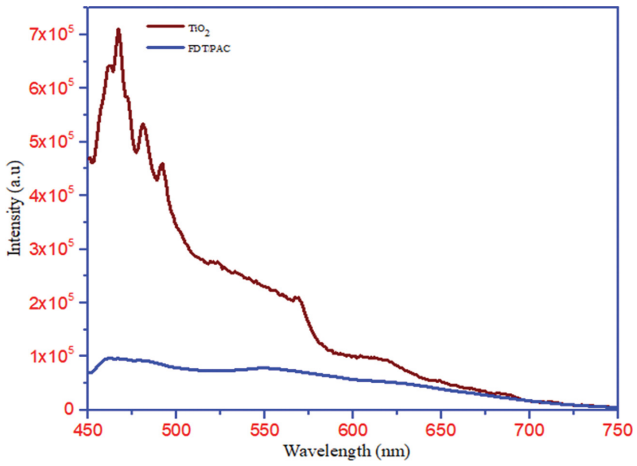

Fig. 5. Photoluminescence spectra of TiO_2 and FDT/PAC nanocomposite.

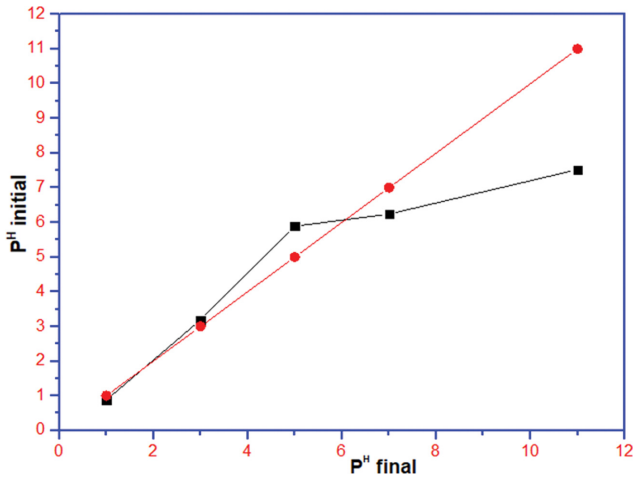

Fig. 6. Zero-point charge plot for FDT/PAC nanocomposite.

Table 1. BET surface area and pore size of TiO_2, FDT/PAC nanocomposite

Proximate analysis (wt%)	
BET surface area (FDT/PAC)	82.779 m^2g^{-1}
BET surface area (TiO_2)	60.21 m^2g^{-1}
BET surface area (PAC)	878.07 m^2g^{-1}
Total pore volume	0.156 cm^3g^{-1}
Pore radius	4.4624 nm

BET surface area and pore volume of a nanocomposite can provide information about the structural properties, pore distribution, and active site's availability for the adsorption of pollutants. The larger the surface area and pore volume of a nanocomposite, the better will be its photocatalytic and adsorption performance. The results for proximate analysis of FDT/PAC nanocomposite are given in Table 1. From the Table it is evident that the FDT/PAC nanocomposite has a large BET surface area compared to pure TiO_2. An increase in the surface area could be due to the incorporation of Fe ions to the TiO_2 complex, which is likely to enhance the stress of the TiO_2 complex [34] and also because of the use of PAC as support propagate surface area of FDT/PAC nanocomposite [28]. The total pore volume of 0.156 cm^3g^{-1} and pore radius of 4.4624 nm gives an idea about the formation of mesoporous material. Thus, higher surface area/active sites should contribute to enhancing the photocatalytic performance of hybrid nanocomposite.

The zero point charge (pH_{zpc}) of the FDT/PAC nanocomposite is found to be 6.02 (Fig. 6), which indicates the surface charge of the nanocomposite will be positive when pH is less than 6.02 and negative when pH is greater than 6.02.

2. Photocatalytic Activity

2-1. Effect of FDT/PAC Nanocomposite Amount

The photocatalytic activity of the FDT/PAC nanocomposite on the degradation of CR dye solution was studied at different dosages of the nanocomposite with different concentration of CR dye solution. The FDT/PAC nanocomposite dosages ranged from 0.02-0.10 g for 20, 60, and 100 ppm of CR solutions (Fig. 7). It can

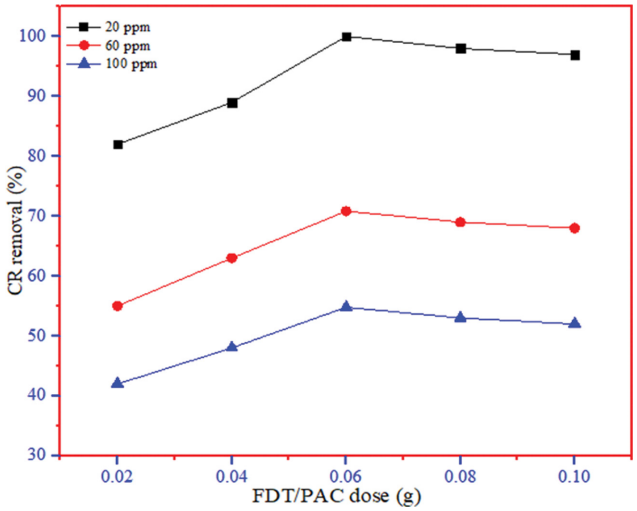

Fig. 7. Effect of FDT/PAC nanocomposite loading in the degradation of CR solution.

be seen that the percentage of degradation of CR was increased with the nanocomposite amount increased. The maximum percentage of degradation (100%) was achieved at 0.06 g of FDT/PAC nanocomposite for 20 ppm CR concentration under the visible light irradiation for 60 mins. There could be several reasons for this result: (i) The addition of PAC increases the surface area of the nanocomposite, helping more CR molecules gathering around FDT/PAC nanocomposite, and (ii) The recombination of electron-hole pair decreases due to the introduction of impurity Fe ions on the TiO_2 matrix. However, when the dose becomes higher than 0.06 g, it serves as a recombination center for the photogenerated electron-hole species, resulting in the decrease in the photocatalytic activity of the nanocomposite. One of the possible explanations could be that when the nanocomposite dose increases beyond a certain dose, the visible light penetration through the reaction mixture becomes lesser due to visible light scattering, hence CR dye degradation efficiency decreases [35]. Thus, for further studies, 0.06 g of FDT/PAC nanocomposite was taken as the optimum amount

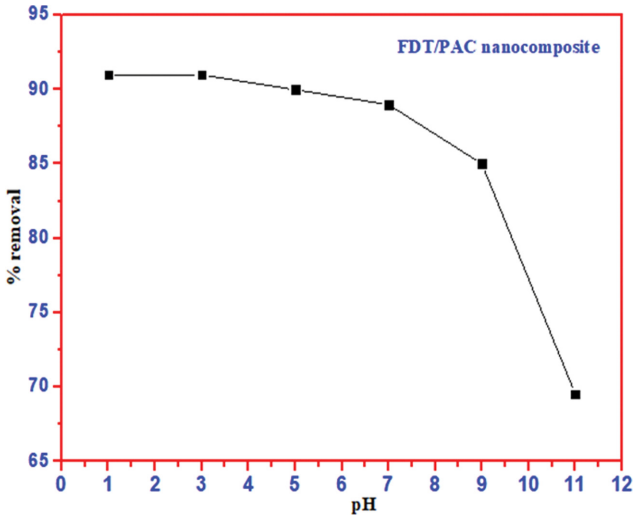

Fig. 8. Effect of pH in the degradation of CR solution.

for CR degradation.

2-2. Effect of pH

The photocatalytic degradation of CR dye was conducted with 0.06 g FDT/PAC nanocomposite with 20 ppm CR dye solution in the pH range of 1-11. From Fig. 8, it is clear that at pH lower than 5, the percentage CR degradation is quite high having maximum degradation at pH 1, which could be due to the positive surface of nanocomposite below its pH_{zpc}. At lower pH (pH 1<pH_{zpc} 6.02), the nanocomposite surface becomes positively charged, i.e., (Fe–TiOH–PAC+H^+↔Fe–$TiOH_2^+$–PAC); thus, the positively charge nanocomposite surface has more electrostatic attraction affinity to bind with negatively charged CR dye, which leads to the maximum degradation of CR dye at pH 1 [36].

2-3. Effect of Initial CR Dye Concentration and Light Irradiation Time

The initial CR dye concentration affects the degradation rate and adsorbent efficiency. Fig. 9(a) shows the effect of initial CR dye concentration with 0.06 g of FDT/PAC nanocomposite at pH=1. The maximum removal of 100% at 60 mins was found for 20 ppm CR dye solution; on the other hand, 88% and 75% was achieved for 60 and 100 ppm solution at 120 mins irradiation. With the increase in the initial CR dye concentration, the number of adsorbed negatively charged CR dye molecules on the positive surface of FDT/PAC nanocomposite prevents the formation of reactive hydroxyl radical due to the deactivation of the active sites of the nanocomposite. Furthermore, at higher CR dye concentration more dye molecules are available for adsorption on the surface of nanocomposite; hence less light will reach the nanocomposite surface, which decreases the rate of formation of hydroxyl and dioxygen radical, thereby decreasing the photocatalytic activity. From Fig. 9 it can also be seen that the percentage removal of CR dye increased with irradiation time and became saturated after exposure to light for 60 mins, and no further removal of dye occurred with further increase in exposure time. This may be due to the formation of a large quantity of small organic molecules produced due to degradation [37]. These small organic molecules adsorb on the surface of the nanocomposite, resulting in the decreased formation of hydroxyl radicals that attack the dye molecules.

For understanding the effect of Fe doping in TiO_2-NP/PAC nanocomposite, experiments were carried out with TiO_2/activated carbon sample without Fe doping under similar sets of conditions (under visible light) and the results are shown in Fig. 9(b). The degradation of 20 ppm CR dye solution was found to be 33.50%, for 60 ppm it was 20%, and for 100 ppm it was 15% as compared to FDT/PAC nanocomposite was 100% degradation for 20 ppm, 70.84% degradation for 60 ppm and 54.80% degradation for 100 ppm of CR dye solution. This partial degradation without Fe doping was probably due to the photosensitive nature of the dye in the visible region. The very high degradation of dye in presence of FDT/PAC catalyst confirms that Fe doping increases the photocatalytic efficiency under visible light. Several researchers [38-40] also reported that some dyes having benzene, naphthalene, anthracene-like structures are photosensitive in the visible region. Even though TiO_2 is not activated by visible light, the dye can also absorb visible light photons, which results in minor degradation of the dye. Further presence of activated carbon which contains some structures similar to the dye enhances the visible light absorption, which

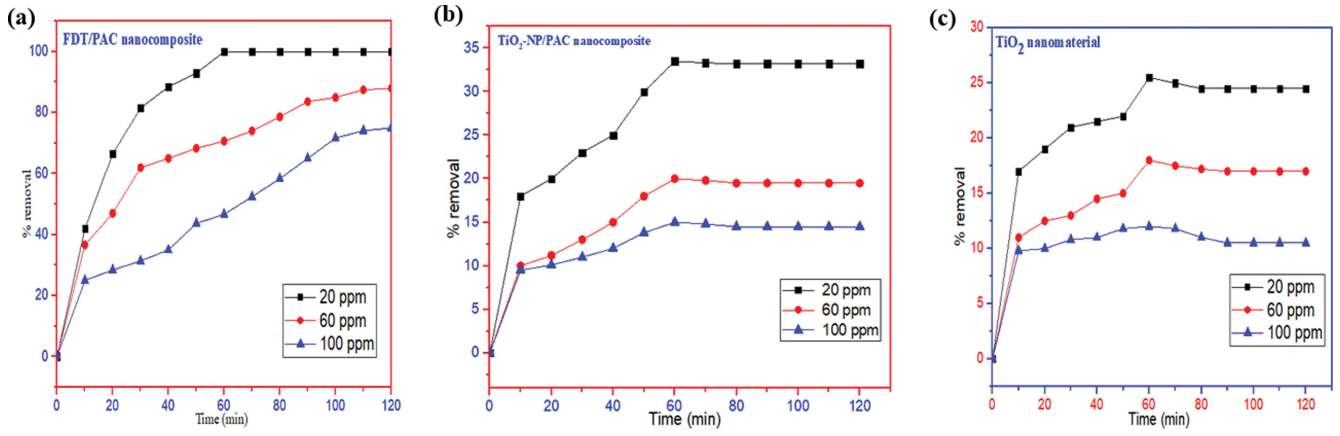

Fig. 9. Effect of degradation of CR dye solutions by (a) FDT/PAC, (b) TiO_2-NP/PAC and (c) TiO_2 catalyst for degradation of different concentration of dye solutions for different contact time under visible light (520 nm).

leads to partial degradation of the dye without TiO_2 activation with Fe ions [41].

Degradation of dye with bare TiO_2 was conducted under similar sets of conditions (under visible light) as represented in Fig. 9(c). From this observation, the bare TiO_2 degradation of 20 ppm CR dye solution was 25%, for 60 ppm it was 18% and for 100 ppm it was 12%. Even though TiO_2 does not show optical response in the visible light region, the dye itself can also absorb visible light photons, which results in partial degradation of the dye at 520 nm due to its photosensitive nature of bare dye.

2-4. Kinetic Studies

Kinetic studies were conducted at optimum conditions, i.e., CR dye concentration of 20 ppm, pH 1, catalyst dose of 0.06 g to understand the rate constant value and efficiency of the nanocomposite in the CR degradation using the Langmuir-Hinshelwood model. The kinetic study was represented using the pseudo-first-order rate Eq. (4) and the half lifetime ($t_{1/2}$) by Eq. (5):

$$\ln\left(\frac{C_o}{C_e}\right) = K_{app}t \tag{4}$$

$$t_{1/2} = \frac{\ln 2}{K_{app}} \tag{5}$$

where C_o is the initial CR concentration (20 ppm); C_e is the CR concentration at equilibrium (0.8 ppm); K_{app} is the apparent rate constant.

The linear plot of $\ln(C_o/C_e)$ versus irradiation time for FDT/PAC nanocomposite gives a high correlation coefficient (R^2: 0.999), which signifies that the CR dye solution degradation follows first-order rate kinetics (Fig. 10). From the slope of the curve, the photocatalytic rate constant K_{app} value was calculated to be 0.05341 min^{-1}, and using Eq. (5) the half-life period was found to be 12.97 min.

2-5. Thermodynamics Studies

In the present study, four temperatures, 298 K, 308 K, 318 K, and 328 K, were used to understand the relationship between changes in temperature with respect to heat and energy. The thermodynamics parameters such as standard entropy (ΔS^o), enthalpy (ΔH^o),

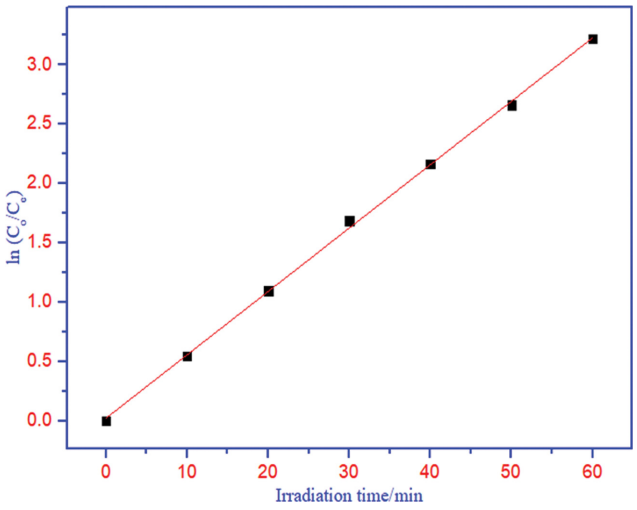

Fig. 10. Pseudo-first-order rate kinetics of CR degradation loaded on FDT/PAC nanocomposite.

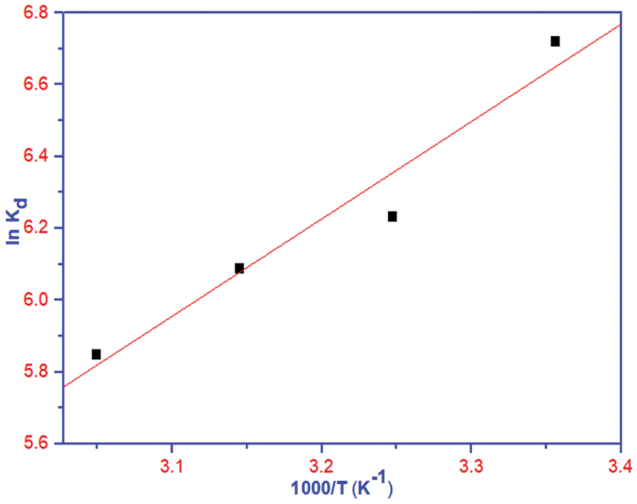

Fig. 11. $\ln K_d$ as a function of 1/T (CR concentration=20 ppm, pH=1, nanocomposite dose=0.06 g and contact time=60 min).

Table 2. Thermodynamic parameters calculated for the degradation of CR dye using FDT/PAC nanocomposite

T (K)	Thermodynamic parameters		
	ΔG^o (kJ mol^{-1})	ΔH^o (kJ mol^{-1})	ΔS^o (J mol^{-1} K)
298	−16.415		
308	−16.301	−19.835	−11.475
318	−16.186		
328	−16.071		

free energy (ΔG^o) of the CR degradation were related to the distribution coefficient (K_d) by:

$$\ln K_d = \frac{\Delta S^o}{R} - \frac{\Delta H^o}{RT} \tag{6}$$

$$\Delta G^o = -RT\ln K_d \tag{7}$$

where T is the absolute temperature, K_d is the distribution coefficient, R (8.314 J mol^{-1} K^{-1}), ΔH^o and ΔS^o are obtained from the slope and intercept by plotting $\ln K_d$ versus 1/T (Fig. 11). Table 2 presents the derived thermodynamics parameters. The negative value of ΔG^o signifies the spontaneity and feasibility of the photocatalytic reaction. Also, the negative values of ΔS^o and ΔH^o signify the randomness in the reaction system, justifying the affinity of FDT/PAC nanocomposite towards CR degradation, which is exothermic.

2-6. Effect of Interfering Ions on CR Photocatalytic Degradation

In the industrial wastewater matrix, CR is found in combination with several ions such as sodium chloride, zinc chloride, copper sulfate, glycine, oxalic acid, sodium nitrite, cadmium nitrate, and EDTA. Hence, to investigate the applicability of FDT/PAC nanocomposite in the industrial wastewater matrix containing CR with several interfering ions was studied by taking 20 ppm interfering ions with an initial CR concentration of 20 ppm, pH at 1, contact time for 60 mins, the temperature at 298 K and 0.06 g of FDT/PAC nanocomposite. The percent removal of CR as a func-

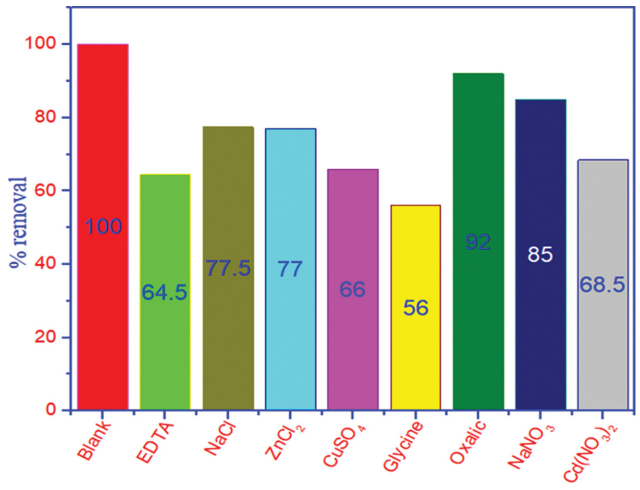

Fig. 12. Photocatalytic degradation of CR in the presence of interfering ions using FDT/PAC nanocomposite.

tion of different interfering ions is presented in Fig. 12. From the figure it can be seen that the percent removal decreases from 100% to 56.0% (Glycine), 64.5% (EDTA), 66.0% ($CuSO_4$), 85.0% ($NaNO_2$), 77.0% ($ZnCl_2$), 77.5% (NaCl), 68.5% ($Cd(NO_3)_2$), 92.0% (oxalic acid). In the presence of glycine (Gly), EDTA, $CuSO_4$ the percentage of degradation of CR decreases significantly because glycine acts as a ·OH scavenger, EDTA as a hole scavenger, SO_4^{2-} as an electron scavenger [42,43]. The presence of chloride ions inhibits the photocatalytic activity of the nanocomposite by scavenging both the ·OH radical and hole, and also blocks the active sites on FDT/PAC nanocomposite [44]. The nitrate ion can absorb light in the UV and visible region; hence there will be fewer photons available towards the pollutant molecules and hence the degradation rate of CR is reduced with the increase of nitrate ion concentration [45]. However, the presence of other ions (oxalic acid, $NaNO_2$) has reduced the effects of the photocatalytic degradation process. From this result, it can be observed that the photocatalytic degradation of CR in the presence of interfering ions follows the order:

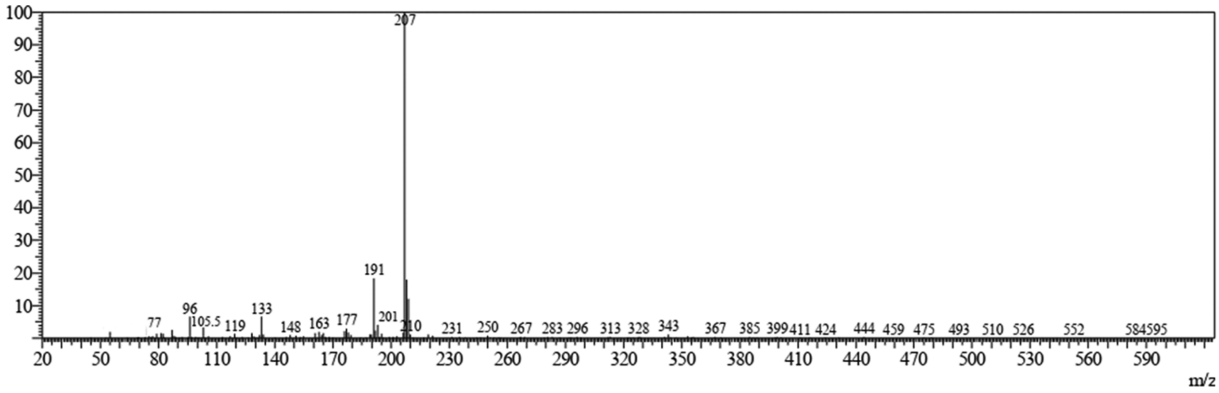

Fig. 13. Mass spectra of the metabolite of CR dye.

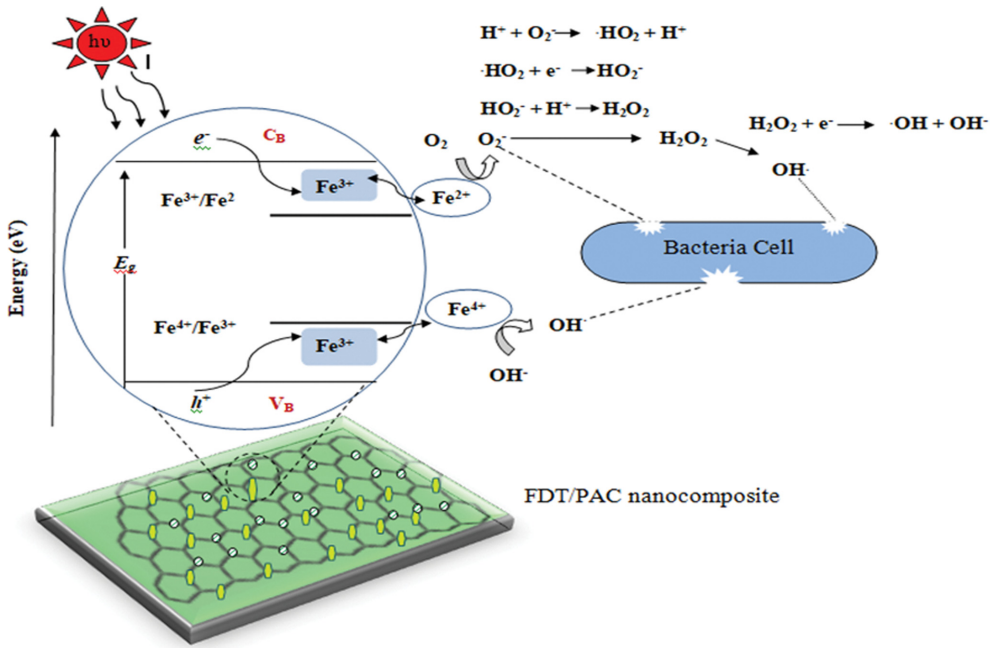

Fig. 14. A schematic diagram showing the mechanism of photocatalytic inactivation of bacteria using FDT/PAC nanocomposite.

Oxalic acid<$NaNO_2$<NaCl<$ZnCl_2$<$Cd(NO_3)_2$<$CuSO_4$<EDTA<Glycine.

2-7. GC-Mass Spectroscopic Analysis of End Products after Degradation of CR Dye

The degraded end products of the CR dye were confirmed using GC-MS analysis and are now included in the text as Fig. 13. Some major and minor products are detected in the GC-MS spectra. The major products corresponding to peak position at m/z=207 are sodium (4-amino-3-diazenyl)-1 napthaoxide, at m/z=191 is 2-diazoniumnapthalene-1, 4-diol, at m/z=133 is succinic acid radical, and at m/z=96 is 2-methyl benzyl cation.

The minor products corresponding to peak position at m/z=177 are 3-diazonium naphthalene-1-ol, at m/z=105.5 is 2-ethyl benzyl cation (IV), and at m/z=77 is phenyl cation (VI).

2-8. Photocatalytic Inactivation

Over the past two decades, photocatalytic inactivation of microorganisms has led to immense applications of this technique for the elimination of microbial contaminants from water [16,46,47]. In the present study, the activity of FDT/PAC, and bare TiO_2 nanomaterial was evaluated for the inactivation of *E. coli* and *S. aureus* under visible light irradiation. Two control experiments were performed: light control (visible light alone without nanocomposite), dark control (0.05 g nanocomposite alone without visible light), and the results are shown in Fig. 16 and 18. From the graph, it is evident that only light (without the nanocomposite) or nanocomposite (without light) cannot inactivate the concerned bacteria [48].

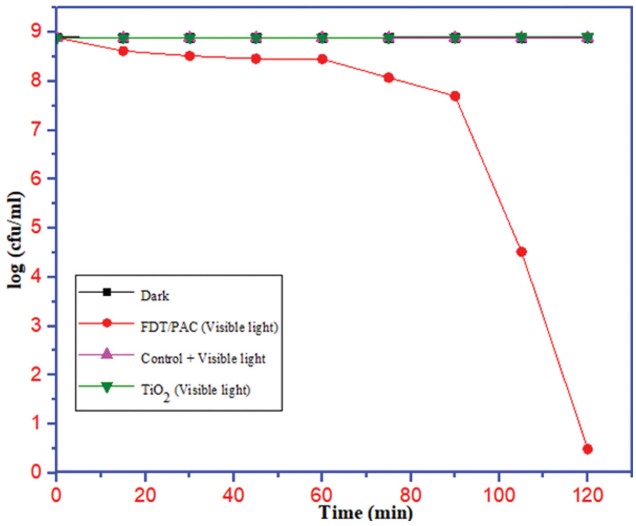

Fig. 16. Photocatalytic inactivation of *E. coli* as a function of time.

Also, bare TiO_2 nanomaterial did not show any antibacterial activity in presence of visible light irradiation. But the inactivation of *E. coli* and *S. aureus* was observed with the FDT/PAC nanocomposite in the presence of light as shown in Fig. 15 and 17. It also signified the photocatalytic inactivation of *E. coli* and *S. aureus* by FDT/PAC nanocomposite with respect to the time within a period of

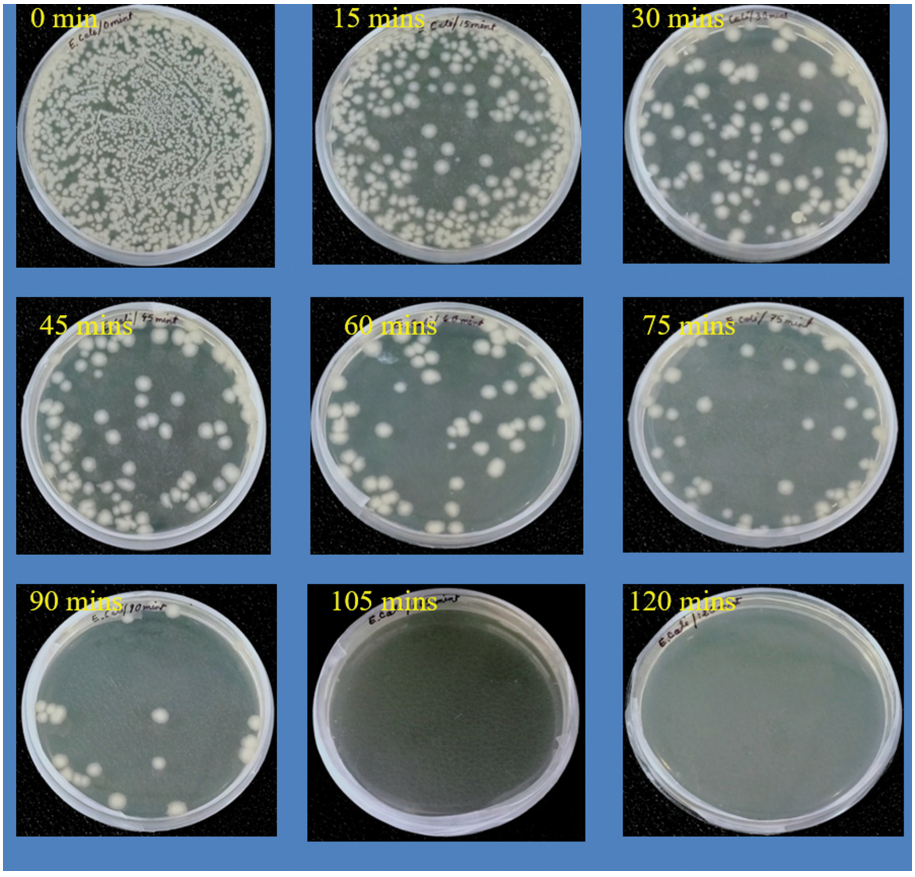

Fig. 15. Photographs of photocatalytic inactivation of *E. coli* at different light exposure times.

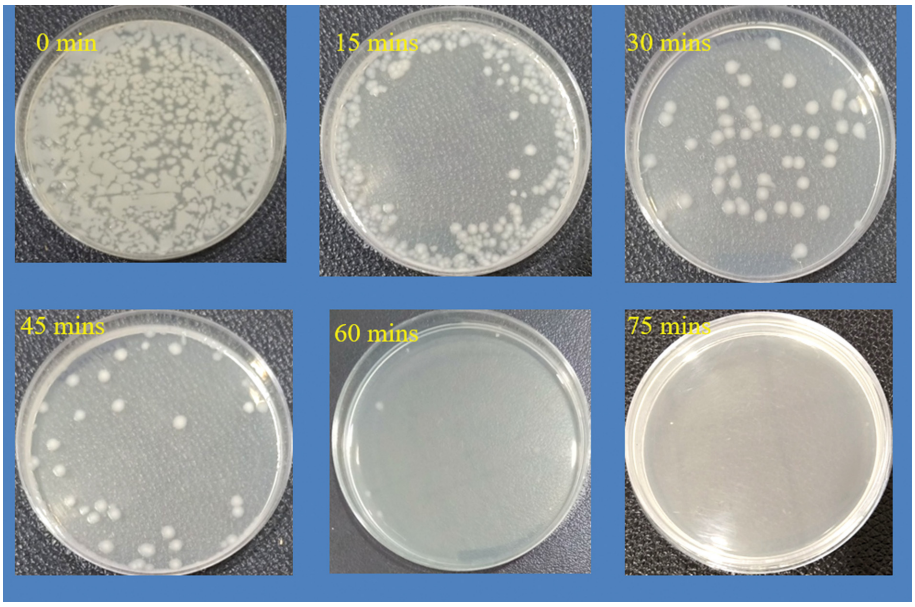

Fig. 17. Photographs of photocatalytic inactivation of *S. aureus* at different light exposure times.

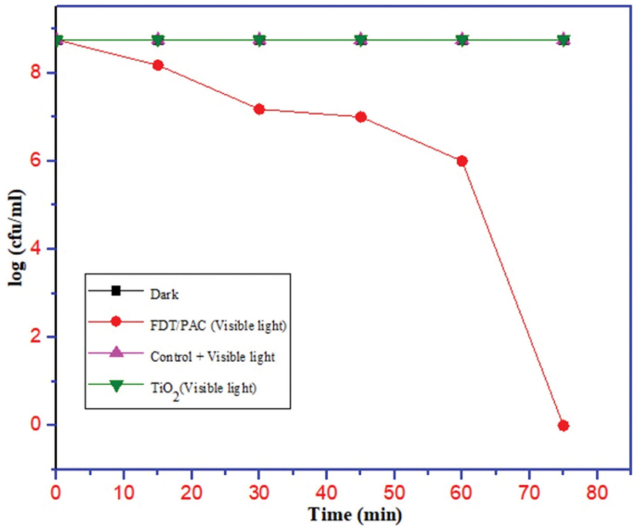

Fig. 18. Photocatalytic inactivation of *S. aureus* as a function of time.

120 mins and 75 mins, respectively. In the photocatalytic inactivation of bacteria, irradiation of light on the FDT/PAC nanocomposite, an electrons and holes pairs were formed which initiated the bacterial inactivation reaction [49]. The Fe doped nanocomposite produces a new higher energy level on the conduction band of TiO_2, the photogenerated electrons (e^-) are excited from the Fe defect state to the TiO_2 conduction band. Due to the efficient trapping of electron-hole pair, more holes (h^+) are formed in the valance band. The photogenerated h^+ can react with adsorbed water molecules and hydroxide ions to form hydroxyl radicals ($^{\cdot}OH$). Thereafter, the electron on the conduction band of TiO_2 combines with the adsorbed water molecules and oxygen ions to produce dioxygen radical ($^{\cdot}O^{2-}$) and this reacts with hydrogen (H^+) ions to form hydrogen peroxide (H_2O_2) and which further generates hydroxyl radicals ($^{\cdot}OH$). The in-situ generated hydroxyl radicals and dioxygen radicals are highly reactive and react with the *E. coli* and *S. aureus* and degrade the cell walls and membranes of the bacteria, leading to the inactivation of bacteria in the manner, which is similar to previous reports (Fig. 14) [50-54].

The Weibull inactivation model was employed to understand the bacterial inactivation mechanism and is given as Eq. (8):

$$\frac{N_t}{N_0} = e^{-Kt} \tag{8}$$

where, N_0 is the initial number of bacteria and N_t is the number of surviving bacteria at time t (min). K is the bacterial disinfection rate constant (min^{-1}) and it is calculated from the slope of the curve [55] and presented in Table 3.

As seen from Table 3, the inactivation rate constant for *S. aureus* is 1.3 times more than for *E. coli*, respectively. This indicates that gram-positive *S. aureus* was more sensitive to photocatalytic inactivation than gram-negative *E. coli*, which is in agreement with previously published reports [56-59]. This could be due to the more complex cell wall structure of *E. coli* than gram-positive *S. aureus*

Table 3. Rate constant of bacterial photocatalytic inactivation of *E. coli* and *S. aureus*

	E. coli	*S. aureus*
Nanocomposite	Rate constant [$k\times10^{-3}$ (min^{-1})]	Rate constant [$k\times10^{-3}$ (min^{-1})]
FDT/PAC+Visible light	66.67	92.2

Table 4. Effect of CR dye concentration on electrical energy consumption

S. No	Experimental conditions			Apparent rate constant (K_{app}) (min^{-1})	R^2	E_{EO} experimental (kWh $m^{-3}order^{-1}$)	E_{EO} model (kWh $m^{-3}order^{-1}$)
	Initial concentration (mg L^{-1})	FDT/PAC concentration (g L^{-1})	pH				
1	20	0.06	1	0.05341	0.99	1,764.69	1,797.41
2	60	0.06	1	0.01854	0.98	5,175.40	5,177.99
3	100	0.06	1	0.01594	0.94	6,007.85	6,022.58

as proposed by Yadav et al. [18]. Gram-positive bacteria have cell walls with thick layers of peptidoglycan, while gram-negative bacteria have cell walls with thin layers of peptidoglycan and contain an outer cell membrane with lipopolysaccharide molecules. Due to the presence of an extra outer cell membrane in gram-negative bacteria, the incorporation of numerous molecules to travel through the cell layer is difficult [58]. Therefore, a greater number of hydroxyl radicals are required to attack the gram-negative bacteria as compared with the gram-positive bacteria for bacterial inactivation.

2-9. Energy Consumption and Cost Analysis

2-9-1. Electrical Energy Determination

The photocatalytic degradation of Congo red dye using visible light irradiated FDT/PAC nanocomposite is an electrical energy-driven process, so accordingly, operating costs are involved. The electrical energy consumed while running the experiment is a major source of operating cost. Therefore, measuring the electric energy per order (E_{EO}) for CR degradation can be a useful and informative way to calculate the expenses during the reaction and it can be calculated as [60]:

$$E_{EO} = \frac{P \times t \times 1{,}000}{V \times 60 \times \log\left(\frac{C_o}{C_e}\right)} \quad (9)$$

where P=Input power (kW), V=Volume of CR (L), C_o=Initial CR concentration, C_e=Final CR concentration, t=Irradiation time (min).

By combining the Langmuir-Hinshelwood pseudo-first-order rate equation (Eq. (4)) with Eq. (9), the E_{EO} for a pseudo-first-order reaction can be written as [61]:

$$E_{EO} = \frac{38.4 \times P}{V \times K_{app}} \quad (10)$$

where K_{app}=pseudo-first-order rate constant (min^{-1}). Eq. (10) was used to calculate the model of electric energy per order for the pseudo-first-order batch reactor.

Table 4 represents the E_{EO} (experimental) and E_{EO} (model) derived values for CR degradation using FDT/PAC nanocomposite. From the table it can be observed that consumption of electrical energy was more for higher CR concentration, which could be due to the absorption of visible light at higher concentration. Experimental E_{EO} value accurately coincides with the kinetic model E_{EO} value, which confirms that the photocatalytic degradation of CR follows pseudo-first-order rate kinetics.

2-9-2. Total Operating Cost

Cost estimation is an important parameter to understand the efficiency of the applied method. It can be measured by adding the total maintenance cost, operating cost, and capital cost. In this study, the total operating cost and energy consumed in CR degradation were calculated using Eqs. (11) and (12) [62]:

$$\text{Total operating cost (INR/Kg)} = \frac{\text{Energy consumed per mg of CR removal (kWh)} \times \text{unit cost (INR/kWh)} \times 10^6}{\text{CR removal (mg)}} \quad (11)$$

$$\text{Energy consumed per mg of CR removal (kWh)} = \frac{\text{Power input (kW)} \times \text{Reaction time (min)}}{1{,}000 \times 60} \quad (12)$$

Table 5 represents the total operating cost involved in the removal of CR from wastewater. It can be noticed that a total of 312.50, 236.74, and 166.67 INR (Indian rupee) operating costs were utilized for 20 ppm, 60 ppm, and 100 ppm CR dye removal using 0.06 g FDT/PAC nanocomposite. These operating costs are mainly dependent on the concentration of CR, amount of nanocomposite, and photocatalytic reactor configuration without considering the cost involved in capital cost and maintenance cost. In Table 5 the total

Table 5. Cost analysis of CR degradation in the photocatalytic reactor under different operating conditions

S. No	Congo red concentration (mg L^{-1}) C_1	FDT/PAC concentration (g L^{-1}) C_2	Congo red removal efficiency (%) C_4	Congo red removal (mg) $C_5=[(C_1\times C_4/100)\times$working volume] C_5	Reaction time (min) C_6	Energy consumed per mg of Congo red removal (kWh) $C_7=[(P\times C_6)/(1{,}000\times 60)]$	Total operating cost (INR/kg of Congo red removal) $C_8=[(C_7\times$unit cost$\times 10^6)/C_5]$
1	20	0.06	100	4	60	0.0005	312.50
2	60	0.06	88	10.56	120	0.001	236.74
3	100	0.06	75	15	120	0.001	166.67

(a) Total energy consumed (P) 0.5 kW [includes energy for electronic magnetic stirrer (50 W), water pump (50 W), exhaust fan (50 W) and Visible lamp (350 W)] (b) Working volume of reactor 0.2 L and (c) Unit cost of power 2.5 INR $(kWh)^{-1}$.

Table 6. Comparison of catalytic activity of previous work in the literature with FDT/PAC nanocomposite

Nanocomposite	Pollutant	Mass ($g\ l^{-1}$)	Volume (ml)	C_o	Contact time (min)	% Removal	Source
Fe-TiO_2/coconut shell AC	Dye wastewater	6	300	-	60	-	[7]
Fe-TiO_2/commercial AC	Reactive Red 198	1	1,000	-	-	-	[8]
Fe-TiO_2/reduced graphene oxide	Rhodamine B	0.6	-	20 ppm	120	91.00	[28]
Fe-TiO_2/zeolite	Methylene blue	1	1,000	20 ppm	60	98.00	[63]
Fe-TiO_2/walnut shells AC	Azo dye	0.25	-	4 mM	240	87.50	[64]
Fe-TiO_2/Zeolites	Methylene blue	1	-	25 ppm	90	92.00	[65]
Fe-commercial AC/TiO_2	Methylene blue	0.10	-	1×10^{-4} M	120	-	[66]
Fe-TiO_2/coconut shell AC	Reactive brilliant red K2G	0.5	200	20 ppm	180	100.00	[67]
Mn, Mo, La/TiO_2/AC	Reactive Red 198	2	-	20 ppm	240	91.00	[68]
FDT/PAC	Congo red	0.06	200	20 ppm	60	100.00	Present study

operating cost decreases from 312.50 to 166.67 INR with an increase in the initial CR concentration.

10. Comparison Studies

In the present study, the efficiency of the present FDT/PAC nanocomposite for photocatalytic degradation of CR was compared with other Fe doped nanocomposite and reported below in Table 6. Although different parameters are used by different authors, yet from the comparative study it can be observed that the present nanocomposite, i.e., Fe doped TiO_2 supported on pinecone activated carbon shows an efficient activity towards Congo red degradation with maximum removal of 100% in 60 mins using 0.06 g of the nanocomposite.

CONCLUSION

Fe doped TiO_2 nanocomposite supported on activated carbon was synthesized using an ultrasonic-hydrothermal method. The characterization results confirmed the presence of Fe ions on the TiO_2 activated carbon nanocomposite. It should be established that doping of Fe^{3+} ions reduced the optical bandgap of the nanocomposite from 3.2 to 2.3 eV. Additionally, activated carbon enhances the surface area and separates the photo-induced electrons and electrons-holes, and inhibits their rapid recombination which extends the electron's life-time and increases the photocatalytic efficiency. The FDT/PAC nanocomposite could be effectively used for the removal of Congo red dye with a maximum degradation percentage of 100% within 60 mins for 20 ppm solution. The thermodynamics study revealed that the degradation process is exothermic and spontaneous. The photocatalytic degradation of CR followed the pseudo-first-order rate kinetics with an apparent rate constant of 0.05341 min^{-1} and a half-life period of 12.97 min, according to the Langmuir-Hinshelwood model. The presence of interfering ions such as glycine, EDTA, $CuSO_4$, $NaNO_2$ affects mostly the degradation efficiency of FDT/PAC nanocomposite in the photocatalytic degradation of CR. The FDT/PAC nanocomposite was very effective in photocatalytic inactivation of bacteria *E. coli* and *S. aureus*, maximum removal of *E. coli* was achieved within 120 mins and *S. aureus* within 75 mins using visible light irradiation. The electrical energy per order (E_{EO}) values was found to be higher for higher concentration of the dye solution. Experimental E_{EO} and model E_{EO} were found to accurately coincide with each other, thereby confirming that the photocatalytic degradation of CR follows pseudo-first-order kinetics. The total operating cost utilized is much less, which is 312.50, 236.74, and 166.67 INR for 20 ppm, 60 ppm, and 100 ppm CR dye removal using 0.06 g FDT/PAC nanocomposite. Thus, the Fe doped TiO_2 activated carbon nanocomposite using visible light irradiation can be a promising photocatalyst for future environmental applications.

ACKNOWLEDGEMENTS

Mridushmita Baruah and Soremo L Ezung, are grateful to the University Grants Commission, New Delhi for the UGC Non-NET fellowship (PF/RDC/NNF-41/2017-1521, PF/RDC/NNF-72/2018-2912) and Aola Supong to the Department of Science and Technology-INSPIRE Fellowship (IF160718). The authors acknowledge the Department of Chemistry, Gauhati University, and CSIR-NEIST, Jorhat for analytical facilities.

CONFLICT OF INTEREST

The authors declare they have no conflict of interest.

REFERENCES

1. K. Kumar and A. Chowdhury, *Encycl. Renew. Sustain. Mater.*, **1**, 949 (2020).
2. A. O. Ibhadon and P. Fitzpatrick, *Catalysts*, **3**, 189 (2013).
3. M. M. Khan, S. F. Adil, A. Al-mayouf and S. F. Adil, *J. Saudi Chem. Soc.*, **19**, 462 (2015).
4. J. Ma, H. He and F. Liu, *Appl. Catal. B Environ.*, **179**, 21 (2015).
5. K. K. Mandari, A. K. R. Police, J. Y. Do, M. Kang and C. Byon, *Int. J. Hydrogen Energy*, **43**, 2073 (2018).
6. M. Khairy and W. Zakaria, *Egypt. J. Pet.*, **23**, 419 (2014).
7. Y. Li, J. Chen, J. Liu, M. Ma and W. Chen, *J. Environ. Sci.*, **22**, 1290 (2011).
8. A. Eshaghi and H. Moradi, *Adv. Powder Technol.*, **29**, 1879 (2018).
9. K. K. P. Rivera, M. D. G. De Luna, T. Suwannaruang and K. Wantala, Int. Conf. Biol. Civ. Environ. Eng., March 27-18, 208 (2014).
10. A. Nishimura, N. Ishida, D. Tatematsu, M. Hirota, A. Koshio, F.

Kokai and E. Hu, *Int. J. Photoenergy*, **2017**, 1 (2017).
11. M. J. Valero-Romero, J. G. Santaclara, L. Oar-Arteta, L. van Koppen, D. Y. Osadchii, J. Gascon and F. Kapteijn, *Chem. Eng. J.*, **360**, 75 (2019).
12. W. Zhou, P. Zhang and W. Liu, *Int. J. Photoenergy*, **2012**, 28 (2011).
13. S. Mohammad, M. Alam, S. K. Sela, A. K. M. Nayab-ul-hossain, M. Masud, K. Sajib and M. R. Hasan, *J. Text. Eng. Fash. Technol.*, **3**, 666 (2017).
14. E. Routoula and S. V Patwardhan, *Environ. Sci. Technol.*, **54**, 647 (2020).
15. J. L. Harry-asobara and I. Kamei, *Appl. Biochem. Biotechnol.*, **189**, 1183 (2019).
16. J. Wang, C. Li, H. Zhuang and J. Zhang, *Food Control*, **34**, 372 (2013).
17. N. K. Eswar, P. C. Ramamurthy and G. Madras, *New J. Chem.*, **40**, 3464 (2016).
18. H. M. Yadav, S. V. Otari, V. B. Koli, C. Kook, S. H. Pawar and S. D. Delekar, *J. Photochem. Photobiol. A Chem.*, **280**, 32 (2014).
19. B. Zhang, S. Zou, R. Cai, M. Li and Z. He, *Appl. Catal. B, Environ.*, **224**, 383 (2018).
20. G. Veréb, L. Manczinger, G. Bozsó, A. Sienkiewicz, L. Forró, K. Mogyorósi, K. Hernádi and A. Dombi, *Appl. Catal. B Environ.*, **129**, 566 (2013).
21. M. Masae and L. Sikog, *Rom. J. Mater.*, **47**, 129 (2017).
22. M. Baruah, A. Supong, P. Chandra, B. Rituparna and K. Chubaakum, *Nanotechnol. Environ. Eng.*, **3**, 1 (2020).
23. H. Teng, S. Xu, D. Sun and Y. Zhang, *Int. J. Photoenergy*, **2013**, 1 (2013).
24. B. M. Babić, S. K. Milonjić, M. J. Polovina and B. V. Kaludierović, *Carbon N. Y.*, **37**, 477 (1999).
25. M. Thakur, G. Sharma, T. Ahamad, A. A. Ghfar, D. Pathania and M. Naushad, *Colloids Surf. B Biointerfaces*, **157**, 456 (2017).
26. S. H. Othman, S. A. Rashid, T. I. M. Ghazi and N. Abdullah, *J. Nanomaterials*, **2011**, 1 (2011).
27. K. Song, S. Lee, C. Y. Suh, W. Kim, K. S. Ko and D. Shin, *Mater. Trans.*, **53**, 2056 (2012).
28. A. A. Isari, A. Payan, M. Fattahi, S. Jorfi and B. Kakavandi, *Appl. Surf. Sci.*, **462**, 549 (2018).
29. S. Sood, A. Umar, S. K. Mehta and S. K. Kansal, *J. Colloid Interface Sci.*, **450**, 213 (2015).
30. H. Belayachi, B. Bestani, N. Benderdouche and M. Belhakem, *Arab. J. Chem.*, **12**, 3018 (2015).
31. T. Daimon, H. Naruse, H. Watanabe, H. Oda and A. Yamanaka, *IOP Conf. Ser. Mater. Sci. Eng.*, **18**, 1 (2011).
32. R. K. Hasibur and K. A. Kumar, *Mater. Sci. Semicond. Process.*, **105**, 104745 (2020).
33. H. Moradi, A. Eshaghi, S. R. Hosseini and K. Ghani, *Ultrason. Sonochem.*, **32**, 314 (2016).
34. X. Li, R. Shen, S. Ma, X. Chen and J. Xie, *Appl. Surf. Sci.*, **430**, 53 (2018).
35. J. M. C. Robertson, P. K. J. Robertson and L. A. Lawton, *J. Photochem. Photobiol. A Chem.*, **175**, 51 (2005).
36. Z. Ghasemi, H. Younesi and A. A. Zinatizadeh, *J. Taiwan Inst. Chem. Eng.*, **65**, 357 (2016).
37. K. Mamun, R. Asw and K. Fahmida, *Appl. Water Sci.*, **7**, 1569 (2017).
38. S. Sood, S. K. Mehta, A. Umar and S. K. Kansal, *Ne. J. Chem.*, **38**, 3127 (2014).
39. S. Kaur and V. Singh, *Ultra. Sonochem.*, **14**, 531 (2007).
40. E. Yun, H. Yoo, W. Kim, H. Kim, G. Kang, H. Lee, S. Lee, T. Park, C. Lee, J. Kim and J. Lee, *Appl. Catal. B: Environ.*, **203**, 473 (2017).
41. A. E. Eliyas, L. Ljutzkanov, I. D. Stambolova, V. N. Blaskov, S. V. Vassilev, E. N. Razkazova-Velkova and D. R. Mehandjiev, *Cent. Eur. J. Chem.*, **11**, 464 (2013).
42. S. Jothivel, R. Velmurugan, K. Selvam, B. Krishnakumar and M. Swaminathan, *Sep. Purif. Technol.*, **77**, 245 (2011).
43. A. Singh, A. Bhati, P. Khare and K. M. Tripathi, *Sci. Rep.*, **9**, 1 (2019).
44. P. Zheng, Z. Pan, H. Li, B. Bai and W. Guan, *J. Mater. Sci. Mater. Electron.*, **26**, 6399 (2015).
45. N. Zhang, G. Liu, H. Liu, Y. Wang, Z. He and G. Wang, *J. Hazard. Mater.*, **192**, 411 (2011).
46. N. R. Srinivasan, P. A. Shankar and R. Bandyopadhyaya, *Carbon N. Y.*, **57**, 1 (2013).
47. S. Boonyod, W. Sutthisripok and L. Sikong, *Adv. Mater. Res.*, **214**, 197 (2011).
48. H. M. Yadav, S. V Otari, R. A. Bohara, S. H. Pawar and S. D. Delekar, *J. Photochem. Photobiol. A Chem.*, **294**, 130 (2014).
49. H. M. M. Ibrahim, *World J. Microbiol. Biotechnol.*, **31**, 1049 (2015).
50. W. Wang, J. C. Yu and P. K. Wong, *Mater. Sci. Forum.*, **734**, 63 (2019).
51. Q. Chen, J. Li, Y. Wu, F. Shen and M. Yao, *Rsc Adv.*, **3**, 13835 (2013).
52. S. Huang, Y. Zhao, H. Xu and H. Li, *Acs. Sustainable. Chm.*, **6**, 11968 (2018).
53. J. Jeong, J. Y. Kim and J. Yoon, *Environ. Sci. Technol.*, **40**, 6117 (2006).
54. M. Karbasi, F. Karimzadeh, K. Raeissi, S. Rtimi, J. Kiwi, S. Giannakis and C. Pulgarin, *Water*, **12**, 1099 (2020).
55. M. T. Taghizadeh, V. Siyahi, H. Ashassi-Sorkhabi and G. Zarrini, *Int. J. Biol. Macromol.*, **147**, 1018 (2020).
56. H. A. Foster, I. B. Ditta and S. Varghese, *Appl. Microbiol. Biotechnol.*, **90**, 1847 (2011).
57. G. Fu, P. S. Vary and C. Lin, *J. Phys. Chem. B*, **109**, 8889 (2005).
58. L. Caballero, K. A. Whitehead, N. S. Allen and J. Verran, *J. Photochem. Photobiol. A Chem.*, **202**, 92 (2009).
59. L. K. Adams, D. Y. Lyon and P. J. J. Alvarez, *Water Res.*, **40**, 3527 (2006).
60. N. Daneshvar, A. Aleboyeh and A. R. Khataee, *Chemosphere*, **59**, 761 (2005).
61. M. A. Behnajady, H. Eskandarloo and M. Shokri, *Dig. J. Nanomater. Biostructures*, **6**, 1887 (2011).
62. M. A. Vishnuganth, N. Remya, M. Kumar and N. Selvaraju, *J. Environ. Manage.*, **181**, 201 (2016).
63. G. Foura, N. Chouchou, A. Soualah, K. Kouachi, M. Guidotti and D. Robert, *Catalysts*, **7**, 1 (2017).
64. R. Nagargoje, S. Atalay, G. A. Ersoz and B. Palas, *Bombay Technol.*, **64**, 45 (2014).
65. H. Taghvaei, M. Farhadian, N. Davari and S. Maazi, *Adv. Environ. Technol.*, **3**, 205 (2017).
66. Z.-D. Meng, K. Zhang and W.-C. Oh, *J. Korean Cryst. Growth Cryst. Technol.*, **19**, 268 (2009).
67. L. I. Youji, L. I. Jing, M. A. Mingyuan, O. Yuzhu and Y. A. N. Wenbin, *Sci. China Ser. B-Chem.*, **52**, 1113 (2009).
68. S. Jorfi, S. Mirali, A. Mostoufi and M. Ahmadi, *Chem. Biochem. Eng. Q.*, **32**, 215 (2018).